www.sciencemag.org/content/348/6242/1486/suppl/DC1

Supplementary Materials for

Factor-dependent processivity in human eIF4A DEAD-box helicase

Cuauhtémoc García-García, Kirsten L. Frieda, Kateryna Feoktistova, Christopher S. Fraser, Steven M. Block*

*Corresponding author. E-mail: sblock@stanford.edu

Published 26 June 2015, *Science* **348**, 1486 (2015)
DOI: 10.1126/science.aaa5089

This PDF file includes:

Materials and Methods

Trapping Assay Assembly

The design of our dumbbell optical trapping assay was similar to that described previously (*31, 32*). Single RNA molecules were transcribed *in situ* and tethered between beads held in each of two optical traps: the 5′ end of the RNA hybridized to a 3 kb DNA handle while the 3′ end of the RNA remained bound to the RNAP; the DNA handle and the RNAP were attached via biotin-avidin linkages to 0.6 and 0.73 μm functionalized beads, respectively.

The RNA transcript contained a large hairpin (72 bp stem and 4 nt loop) with 50 or 75% A:U content, as shown in **Figures 1A** and **S1**. A 20 nt single-stranded "target" RNA region was present on the 5′ side of the hairpin, which allowed for upstream binding of eIF4A (15 nt footprint) alone, or bound to different combinations of initiation factors. Similarly, an approximately 7 nt single-stranded RNA region extended from the 3′ end of the RNA hairpin to the RNAP: this region was kept short to prevent efficient eIF4A loading at the 3′ end of the hairpin (*22*).

The eIF4A helicase and other initiation factors were purified as described previously (*33*). Experiments were carried out in 20 mM Tris-acetate, 100 mM KCl, 2 mM Mg-acetate and 1 mM DTT at 25ºC. The buffer was supplemented with an oxygen-scavenging system consisting of glucose oxidase and β-D-glucose. Unless otherwise stated, the eIF4A helicase concentration was maintained at 1 μM, which is comparable to the K_D for eIF4A and the initiation factors eIF4B, eIF4H and eIF4G$_{682\text{-}1105}$ (see below). Different factor combinations with eIF4A were formed by adding stoichiometric amounts of eIF4B, eIF4H and/or eIF4G$_{682\text{-}1105}$. The ATP-Mg concentration was 1 mM (standard data collection) or 0 mM (controls).

Data Collection

Data acquisition rates ranged from 2-20 kHz, as appropriate for the experiment, with low-pass Bessel filtering at half that frequency (Nyquist rate). Custom software was used for data collection (written in LabVIEW) and analysis (written in IGOR Pro). The instrument can be operated in one of two measurement modes: ramped force or constant force. Constant-force measurements are implemented using active feedback to maintain the bead position with respect to the trap center; video tracking was used simultaneously to maintain a constant *z*- (axial) position. The constant-force mode was used to acquire all data shown here, including the equilibrium measurements of RNA structures and the detection of helicase activity (*31, 32*).

Supplementary Text

Observations of eIF4A and its complexes were collected in the single-molecule regime

To ensure that a single helicase was bound to the RNA tether, we performed controls with different concentrations of eIF4A helicase at a constant RNA concentration (13 pM) in the dumbbell optical trapping assay. At eIF4A concentrations of 1 μM or below, we rarely observed eIF4A-dependent unwinding activity in the assay, and no activity below 0.5 μM. To corroborate this finding, we estimated the probability of finding a single eIF4A helicase bound to an RNA tether under our experimental conditions.

The probability, P_b, of having a helicase bound to the RNA is estimated by:

$$P_b = \frac{RA}{R_T}$$

and

$$RA = \frac{K_D + R_T + A_T - \sqrt{(K_D+R_T-A_T)^2 + 4K_D A_T}}{2}$$

where RA, R_T and A_T are the concentrations of bound RNA, total RNA and total eIF4A helicase, respectively, and K_D is the dissociation constant. Previous studies have shown that eIF4A affinity for RNA is a function of how much ssRNA is accessible: the eIF4A binding affinity increases significantly as the single stranded region of the RNA increases from 4 to 15 nt to accommodate the helicase footprint, with little additional change observed from 15 to 20 nt (K_D ~ 13 μM for 20 nt ssRNA) (*22*). In our initial RNA tether (with the reporter hairpin closed and a 20 nt ssRNA landing region available), the probability of having a single helicase bound was 0.07 (**Fig. S2A**). This result suggests that less than 1 in 10 tethers in our assay has a molecule of helicase bound to it. The probability of finding two helicase molecules bound (assuming these are independent events, and sufficient ssRNA is available to make room for a second helicase) is roughly P_b^2 ~ 0.005, i.e., once in every 200 tethers.

Complexes with eIF4A have a greater RNA affinity, and thus a higher probability of binding. As a representative example, the complex eIF4A•B•$G_{682\text{-}1105}$, has increased affinity via the RNA binding domains of eIF4B and eIF4G. Its apparent K_D is 127 nM, based on an unwinding titration assay (**Fig. S2B**), which is similar to that reported previously for the complex with full length eIF4G (K_D = 367 nM) (*33*). With a tighter K_D, the nominal RNA binding probability of eIF4A•B•$G_{682\text{-}1105}$ is somewhat higher in bulk assays, but it is still subsaturating (**Fig. S2**). However, the effective probability of RNA binding is significantly lower in single-molecule assays, because it is driven by losses of proteins that can adhere to the interior glass surfaces of the microscope flow cell, which has a high surface-to-volume ratio (internal volume is ~5 μL). This results in greatly reduced concentrations delivered, as evidenced by the nearly complete loss of unwinding activity, as well as binding events, at nominal concentrations much below 1 μM (**Fig. S6**). Additional evidence of protein adhesion comes from the observation that the functionalized (e.g., with nucleic acids) polystyrene beads used in assays stick readily to one another, and to glass flow cell surfaces, once initiation factors are introduced.

Finally, we note that the minimal useable concentration of eIF4A•B•G in our assays is bounded, because the initiation factors must be present at a sufficiently high concentration to form a stable complex. Exact values for the association of eIF4A•B•G are not available, but one can estimate this affinity to be ~250 nM, based on previous estimates of the pairwise binding constants between the factors (*10, 11, 33*)**.** Most of our single-molecule experiments were carried out at 1 μM, which is near the lower limit for complex association.

<u>eIF4A is required for double-stranded unwinding activity</u>

Complexes with eIF4A exhibit step behavior as they unwind dsRNA (**Fig. 2 and Fig. S3**). Control tests for single-molecule unwinding activity for single and duplex factor combinations in the absence of eIF4A showed no unwinding behavior (**Fig. S4**).

The overall mean rate of unwinding was calculated for different complexes with eIF4A (**Fig. S5**). Estimates represent the average ratio of the net base pairs unwound to the corresponding time required for that unwinding. (Estimates do not include any final hairpin opening events, as this unwinding was mediated by force at the point where the ever-shortening hairpin could no longer sustain the applied load.) eIF4A alone as well as duplexes with eIF4A have very low mean rates of progression through the RNA hairpin reporter, as they achieve only limited unwinding and have long pauses between steps. The mean rates for eIF4A•B•G and eIF4A•H•G, which show progressive unwinding, are more meaningful: eIF4A•B•G proceeds the fastest overall at ~4.6 bp/s under our experimental conditions. (Note that the time for opening base pairs during an unwinding event is instantaneous on our timescale (millisecond); mean rates here are longer due to pausing between steps.)

<u>eIF4A•B/H•G complexes proceed predominantly via a processive rather than a distributive mechanism</u>

Unwinding could, in theory, proceed by either a processive or a distributive mechanism (i.e., unwinding could occur by a single complex taking successive steps or by successive binding events of multiple complexes, respectively). There are four lines of reasoning that argue that the mechanism of unwinding for eIF4A•B/H•G complexes must be processive, and not distributive:

1) ***Argument by arrival time.*** The arrival time, defined as the mean time before unwinding is observed in our assays subsequent to the addition of enzyme in the flow cell, is ~29 s for eIF4A•B•G, and it's even longer for eIF4A alone, at ~69 s (**Table S1**). Because these arrival times already exclude the time required for buffer replacement (~5 s), the delays are attributable to the time required for eIF4A (and/or its complexes) to locate its ssRNA target by diffusion at the low concentrations used in our assays, bind, and begin unwinding. Therefore, if a molecule of eIF4A (or a complex thereof) were to either dissociate or move downstream of the ~20-nt "landing zone" of ssRNA, freeing it up, one would expect a time interval averaging ~29 s or so (depending upon the complex) before another eIF4A complex could arrive and bind. In a distributive mechanism, this would result in the unwinding steps (11 bp) being separated by lengthy pauses, lasting an average of 29 s or more, *which is contrary to observation*. Instead, the 72-bp reporter hairpins were completely unwound (in multiple steps) by eIF4A•B•G in times of ~10 to 40 s, with any pauses lasting just a few seconds, at most. The single-molecule records can only be explained if the unwinding complex remains continuously bound to the substrate, ruling out a distributive mechanism.
2) ***Argument by re-annealing.*** The single-molecule data not only show that eIF4A alone is non-processive, but also shows that the RNA hairpin, once unwound in a single step by ~11 bp, can re-anneal instantly on the timescale of our measurements, i.e., within a few milliseconds (**Fig. 2** and **Fig. S3**). This same, instantaneous RNA re-annealing is also observed for complexes with eIF4B, eIF4H, and eIF4G. In a distributive mechanism, one would expect to see comparatively high numbers of backsteps for all complexes, as the multiple copies of the helicase became transiently bound and unbound. Instead, the single-molecule unwinding traces for eIF4A•B•G and eIF4A•H•G displayed few, if any, re-annealing events.

3) ***Argument by binding affinity.*** Based on bulk measurements of the apparent dissociation constant, K_D (**Fig. S2B**), the probability of eIF4A being bound to the RNA substrate is quite low, but the probability of eIF4A•B•G binding is notably higher. Nevertheless, the experimentally relevant probability of eIF4A•B•G binding remains fairly low in single-molecule assays, driven by protein losses due to sticking to the glass surfaces of the flow cell, which greatly reduce the delivered concentrations, as evidenced by the loss of unwinding activity, as well as binding events, at even slightly lower concentrations than those employed for most of these assays (**Fig. S6**).

   In a distributive mechanism, highly probable, successive binding events are necessary to drive duplex unwinding. In such a case, we might expect to see unwinding events even in the absence of ATP, for example in the presence of the non-hydrolyzable ATP homolog (AMP-PNP), but this is contrary to observation. Furthermore, the binding affinity of eIF4A•B•G is expected to be similar in the presence and absence of ATP, because the affinity of eIF4A changes less than 10-fold under such circumstances (*21, 34*). These facts also argue against a distributive mechanism.

   Some previous work has, indeed, reported the full unwinding of short duplexes even in the absence of ATP (*15*). However, while binding events could occur in the absence of ATP in our assays, they did so very infrequently (i.e., typically on timescales longer than the mean arrival times for factors), and these were never observed to open the reporter hairpin completely.

4) ***Argument by concentration independence.*** In a distributed mechanism, unwinding occurs through the successive binding of multiple copies of helicase. Therefore, the rate of unwinding is proportional to the concentration of the helicase. By contrast, in a processive mechanism, the binding of a single molecular complex results in a large number of turns being unwound in succession. The hallmark of a processive mechanism is that the rate of unwinding is *independent of the enzyme concentration in the limit of low concentration*. When enzyme levels were reduced to 0.5 μM, which is half our usual experimental concentration (1 μM), this yielded little or no unwinding activity, because RNA binding became vanishingly improbable, indicative of the single-molecule limit. In a distributive mechanism, by contrast, reducing the enzyme concentration by a factor of two should have halved the unwinding rate, not abolished it (**Fig. S6**). We also collected data at twice the experimental concentration of eIF4A•B•G (at 2 μM). Under these conditions, the observed unwinding rate was the same within statistical error—and not doubled—and the single-molecule records were all qualitatively similar (**Fig. S7**). Furthermore, when unwinding activity was assayed using eIF4B•G at 2 μM in conjunction with eIF4A at 0.5 μM, the unwinding rate was similar to data obtained in conjunction with 1 μM eIF4A. Therefore, over a four-fold range in helicase concentration, the activity (once bound to RNA) was similar, and this is indicative of a processive mechanism.

Overall, the activity of eIF4A•B/H•G in single-molecule assays leads to processive unwinding. This finding does not imply that some form of distributive binding cannot also operate under different conditions, and it might conceivably be a mechanism for unwinding by eIF4A alone, or in complexes, but at significantly higher concentrations, or over timescales much longer than those observed here for unwinding. That said, we find that eIF4A is able to operate processively in conjunction with its co-factors.

eIF4A and HCV NS3 helicases translocate with a similar step size

The hepatitis C virus NS3 DEAD-box helicase translocates 11 ± 3 bp (mean ± SEM) per step, with substeps measuring 3.6 ± 1 bp (mean ± SEM). The step size similarity between the NS3 and eIF4A helicases is likely attributable to their structural similarity: RecA-like domains 1 and 2 of NS3 are superimposable on the homologous NTD and CTD domains of eIF4A, respectively (**Fig. S10**) (1). Interestingly, in NS3, a single residue, tryptophan 501, is thought to prevent the enzyme from slipping backwards, allowing 3′-to-5′ translocation. However, eIF4A is believed to translocate during scanning with opposite directionality and lacks a structural homolog of this residue (**Fig. S10**) (2, 3).

eIF4B, eIF4H and eIF4G$_{682\text{-}1105}$ promote eIF4A directional translocation

We counted all the forward and backward steps taken by the helicase from the beginning of translocation until dissociation from the RNA template, i.e., during full refolding of the template or complete melting of the hairpin. Probabilities were calculated for either taking a step forward, $P_+ = n_+/(n_+ + n_-)$, or backward, $P_- = n_-/(n_+ + n_-)$, where n_+ and n_- are the total numbers of forward and backward steps, respectively. The ratios of forward to backward stepping probabilities, P_+/P_-, for different factors complexed with eIF4A are reported in the main text and **Figure 3A**.

A graphical representation of the directional stepping dynamics of eIF4A and factor combinations is shown in **Figure S11**. Each point shows the correlation between step size and direction for a pair of consecutive steps, where the *x* axis represents $step_n$ and the *y* axis represents $step_{n+1}$. The point distribution for eIF4A was concentrated in the second and fourth quadrants, corresponding to successive forward and backward steps being taken. The binding of eIF4A to initiation factors eIF4B, eIF4H, or eIF4G$_{682\text{-}1105}$ did not strongly alter these dynamics. However, the complexes eIF4B•G$_{682\text{-}1105}$ and eIF4H•G$_{682\text{-}1105}$ shifted the pairwise step distribution into the first quadrant, consistent with more consecutive forward steps, and to directional translocation of the corresponding complexes. Based on our assay geometry, in which translocation can only initiate from the 5′ side of the reporter hairpin, this processive stepping is believed to proceed in the 5′-to-3′ direction.

eIF4A translocates as a Markovian system, alone or bound to other factors

We assessed whether each translocation step of eIF4A, alone or bound to different factor combinations, was an independent event or correlated with previous steps, i.e., whether or not the system displayed the Markov property (**Fig. S13**). The probability of observing two consecutive forward steps for any given factor combination was estimated as $P_{++} = n_{++}/(n_{++} + n_{+-} + n_{-+} + n_{--})$, where n_{++}, n_{+-}, n_{-+} and n_{--} represent the number of instances of two consecutive forward steps, a forward followed by a backward step, a backward followed by a forward step, and two consecutive backward steps, respectively. Analogously, we estimated the probabilities P_{+-}, P_{-+} and P_{--}. The ratio $(P_+)^2/P_{++}$, with P_+ being the probability of taking a single forward step, describes whether two consecutive forward steps are correlated. We also computed the ratios P_+P_-/P_{+-}, P_-P_+/P_{-+} and $(P_-)^2/P_{--}$, corresponding to the different possible combinations of steps (*35*). All these ratios were near unity, suggesting that there is little or no correlation between any two consecutive steps, irrespective of the direction of movement.

Randomness analysis suggests a single rate-limiting step in the translocation of eIF4A and different factor combinations

Analysis of the relative forward and backward stepping probabilities for eIF4A, alone or in complexes, indicates that it translocates in a Markovian fashion. That is, the decision to take a forward or backward step is uncorrelated with the direction of the previous step, and there is no apparent memory associated with any given sequence of steps (**Fig. S13**). Further, a metric that reflects the number of rate-determining transitions in the underlying reaction cycle, the randomness parameter (*36*), was close to unity for eIF4A both alone and in complexes, suggesting that the translocation mechanism is governed by a single rate-limiting step, a finding supported by previous bulk biochemical studies (*21, 34*) (**Fig. S14**).

To assess whether binding of accessory factors changes the number of rate-determining steps in the translocation of eIF4A, we calculated the randomness parameter, *r*. This parameter is a dimensionless measure of the second moment of the step-time distribution (*27*). For a process in which all the step times are equal, $r = 0$; conversely, for a Poisson process in which the step times follow an exponential distribution, $r = 1$. The inverse of the randomness parameter, r^{-1}, can be interpreted as the number of rate-determining steps in a biochemical pathway (*27*). In a process where all transitions are Markovian, the randomness will have contributions from both the variability of the step time, $r_{step\ time}$, and the step size, $r_{step\ size}$, given by (*36*):

$$r = r_{step\ time} + r_{step\ size} = \frac{\langle \tau^2 \rangle - \langle \tau \rangle^2}{\langle \tau \rangle^2} + \frac{\langle d^2 \rangle - \langle d \rangle^2}{\langle d \rangle^2}$$

where $\langle \tau \rangle$ and $\langle d \rangle$, and $\langle \tau^2 \rangle$ and $\langle d^2 \rangle$, are the first and second moments of the step time and step size distributions, respectively. We found that, irrespective of the factor combination, the randomness was approximately one (**Fig. S14**). This suggests that 1) there is a single rate-limiting step in the translocation of eIF4A, and 2) the complexes formed between eIF4A and additional factors also translocate with a single rate-limiting step.

eIF4A•B•G$_{682\text{-}1105}$ or eIF4A•H•G$_{682\text{-}1105}$ pausing does not appear to be correlated with the location of the start codon

In many biochemical systems, a direct correlation has been shown between macromolecular pausing and gene regulation (*37, 38*). In the case of ribosomal scanning, it has been suggested that pausing should occur in regions containing initiation codons, perhaps as a consequence of the AUG recognition process, or of gene regulation in general (*39*). As discussed previously, eIF4A and all factor combinations produced a series of long pauses on the hairpin stem, separated from one another by approximately 11 bp (i.e., one helical turn). Although the hairpin stems contain several instances of AUG, we found no correlation between pausing and the locations of such start codons (**Fig. 3C**, red rectangles). Therefore, although eIF4A, eIF4B, eIF4H and eIF4G$_{682\text{-}1105}$ are responsible for processive translocation and mRNA unwinding, they do not seem to participate directly in AUG recognition, at least in the absence of other initiation components.

Because successful gene expression requires correct identification of the start site during scanning, additional components likely comprise the anticipated "proof-reading" mechanism that is believed to span approximately three to ten bases (*40-43*). Yeast studies suggest that the discriminatory mechanism identifying the initiation codon may be mediated by the 40S ribosomal subunit, eukaryotic initiation factors 1, 1A, 5, and Met-tRNA$_i^{Met}$ (*44*). Though some

components involved in AUG recognition have been identified, there is still much to learn about how preinitiation complex pausing is achieved and influences gene regulation.

eIF4A can unwind mRNA by mass action

The lack of intrinsic processivity for eIF4A, together with the recent discoveries of additional helicases that participate in scanning, has led to the hypothesis that eIF4A's role is to melt local UTR regions by mass action (*9*). It has been reported that eIF4A can sequentially bind and melt RNA secondary structure, even in the presence of the non-hydrolyzable analog ATP-BeF_x (*15*). In our single molecule assay, we observed that a processive complex is formed by eIF4A•B•$G_{682\text{-}1105}$ or eIF4A•H•$G_{682\text{-}1105}$ in the presence of ATP. However, when the concentration of eIF4A alone was increased (3-5 μM; with or without ATP) to a level where multiple helicases could bind a single RNA tether, then partial melting of the hairpin—presumably, mediated by sequential helicase binding events—was occasionally observed. This behavior resembles that of ribosomal protein S1, which can unwind structured RNA and thus facilitate ribosome docking (*45*). Therefore, although a mechanism for RNA melting that involves mass action (i.e., binding alone) is possible in this system, it is inefficient compared to melting by eIF4A•B/H•$G_{682\text{-}1105}$, which can take place at lower factor concentrations. Nevertheless, the identification of eIF4A•B/H•$G_{682\text{-}1105}$ as a processive complex does not rule out the additional possibility that multiple eIF4A molecules might indeed bind and restructure 5′ UTRs within the cell.

Single-molecule data trends are comparable to bulk findings

The single-molecule experiments described here were carried out in conditions analogous to those previously used for bulk studies of eukaryotic initiation factors (*19, 33*). Further, the truncation mutant of eIF4G used here, eIF4G$_{682\text{-}1105}$, has been previously characterized and successfully used in reconstituted bulk assays (*33*). The trends in enhancement of eIF4A activity by other initiation factors noted in these previous works, as well as those of other researchers (*12, 19, 23-26, 33, 46-48*), are successfully recapitulated in our single-molecule studies, but now with insight as to how this enhancement is achieved and the nature of the resulting processive motion.

To verify that our results were not specific to the use of truncation mutant eIF4G$_{682\text{-}1105}$, we used a bulk, fluorescence-based unwinding assay to assess unwinding activity with full length eIF4G$_{wt}$ (*19, 33*). (Note that eIF4G$_{wt}$ was assayed with eIF4E because eIF4G$_{wt}$ retains the autoinhibitory eIF4E binding site and requires this cofactor to have full activity (*19*)). The results with full length enzyme (eIF4G$_{wt}$; **Fig. S15**) and truncation mutant (eIF4G$_{682\text{-}1105}$; (*33*)) were similar, indicating that use of eIF4G$_{682\text{-}1105}$ in our assays does not affect our conclusions regarding processivity. Specifically, for example, full length eIF4G alone cannot convey processivity to eIF4A; the triplex eIF4A•B•G is required.

Supplementary Figures

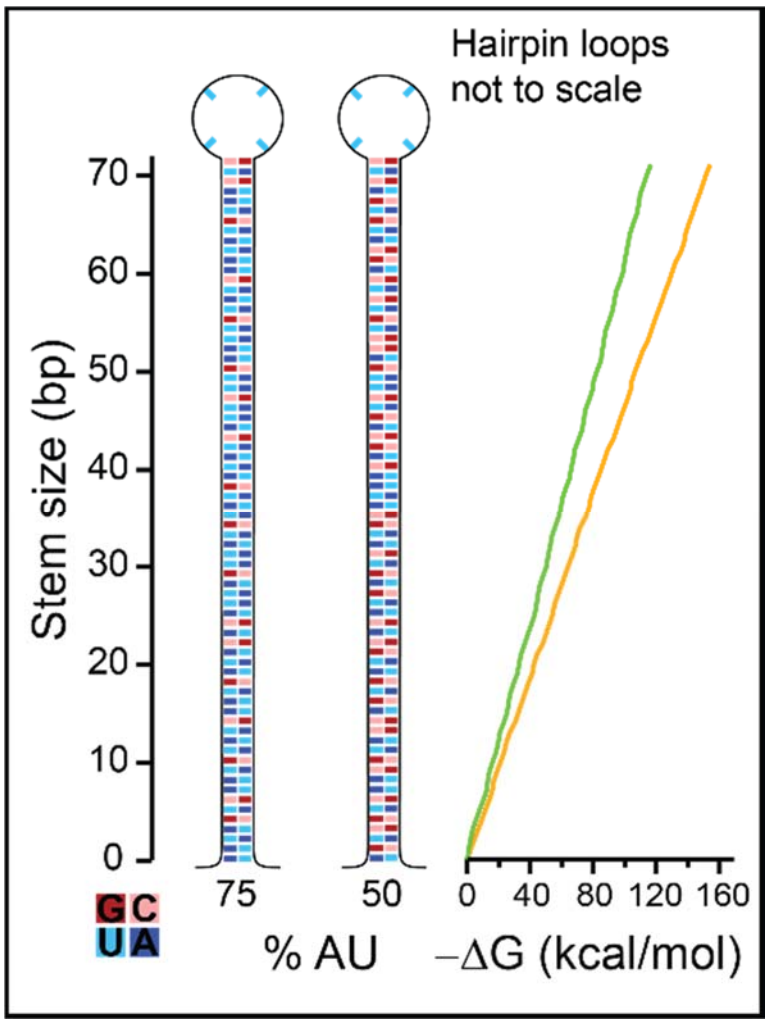

Fig. S1. Reporter hairpins.

The figure illustrates the reporter hairpins used in this study and their energy landscapes. Both hairpins contain a 72-bp stem and a 4-base loop, but differ in stem AU content (50 and 75% AU). Differences in AU content are reflected directly in hairpin stabilities, which were calculated (using mfold) to be -152.2 and -114.7 kcal/mol for the 50% and 75% AU hairpins (yellow and green energy landscapes), respectively (*49*). The 4-nt loop at the top of the hairpin was introduced to stabilize the hairpin, because GNRA tetraloops are stabilized via base stacking interactions, and to be small enough to prevent eIF4A loading to the loop RNA.

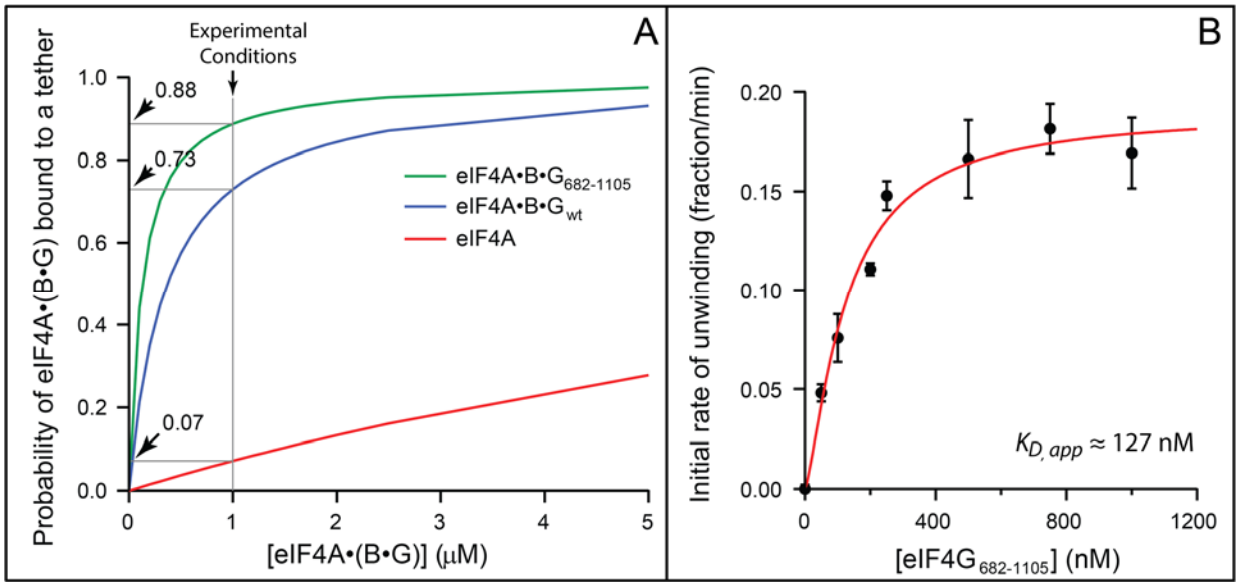

Fig. S2. Measured binding affinities of eIF4A and complexes.

(A) Probability of eIFA•(B•G) being bound to a single, initial RNA tether as a function of concentration. The figure shows estimated binding isotherms of eIF4A, eIF4A•B•G_{wt} and eIF4A•B•$G_{682\text{-}1105}$ (red, blue, and green, respectively). Binding isotherms were calculated using K_D values of 13 μM, 367 nM and 127 nM, corresponding to eIF4A, eIF4A•B•G_{wt}, and eIF4A•B•$G_{682\text{-}1105}$, respectively (*19, 22*). Under our experimental conditions, eIF4A present alone will bind only ~1 in 10 RNA tethers. The eIF4A•B•$G_{682\text{-}1105}$ complex has a higher, but still subsaturating, RNA binding probability in bulk solution. The effective concentration inside the flow cell used for single-molecule assays is reduced, however, due to protein loss (see text). **(B)** A bulk, fluorescence-based unwinding assay was used to obtain initial rates of helicase unwinding (expressed as a fraction of RNA duplex unwound per minute) as a function of varied eIF4G$_{682\text{-}1105}$ concentration in the presence of 1 μM eIF4A and 1 μM eIF4B (*19, 33*). Data were fit to the Hill equation as described in (*19*) and imply an apparent dissociation constant ($K_{D,app}$) of 127 ± 21.5 nM for eIF4A•B•$G_{682\text{-}1105}$ from RNA. This affinity is similar to that reported previously for a comparable eIF4A•B•G_{wt} complex: $K_{D,app}$ = 367 ± 115 nM (*19*). All reactions containing eIF4G$_{wt}$ also contained a stoichiometric amount of eIF4E. Initial rates are shown as means of three independent experiments ± SEM.

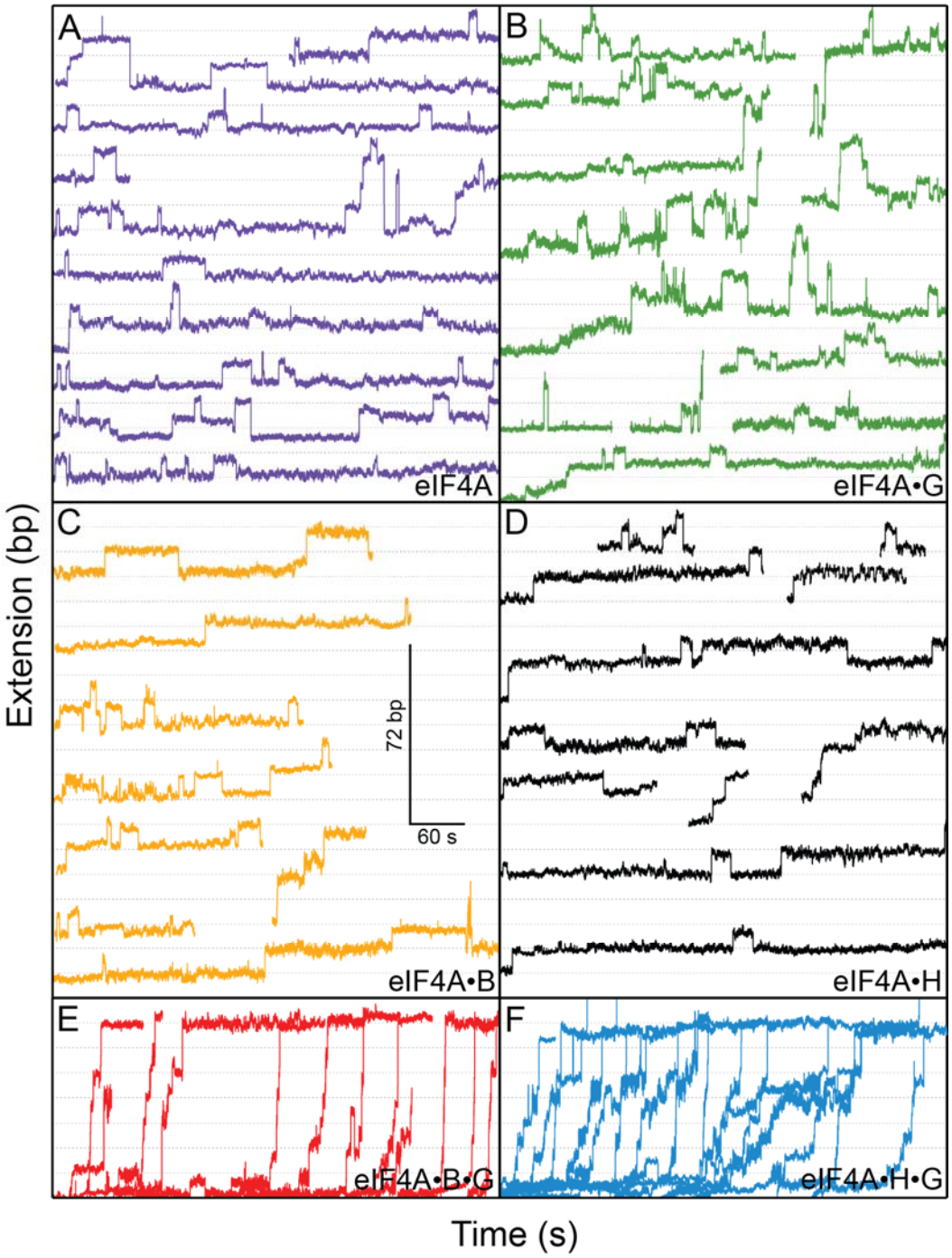

Fig. S3. Representative traces for eIF4A and factor combinations.

Representative single-molecule traces of eIF4A (purple, (**A**)), eIF4A•$G_{682\text{-}1105}$ (green, (**B**)), eIF4A•B (yellow, (**C**)), eIF4A•H (black, (**D**)), eIF4A•B•$G_{682\text{-}1105}$ (red, (**E**)) and eIF4A•H•$G_{682\text{-}1105}$ (blue, (**F**)) obtained with the optical trapping assay; traces are offset vertically and horizontally for clarity. Horizontal grid lines correspond to 10 bp, and the total observation time represents 500 s. ("eIF4G" corresponds to the truncation mutant $eIF4G_{682\text{-}1105}$ in all figures unless otherwise specified).

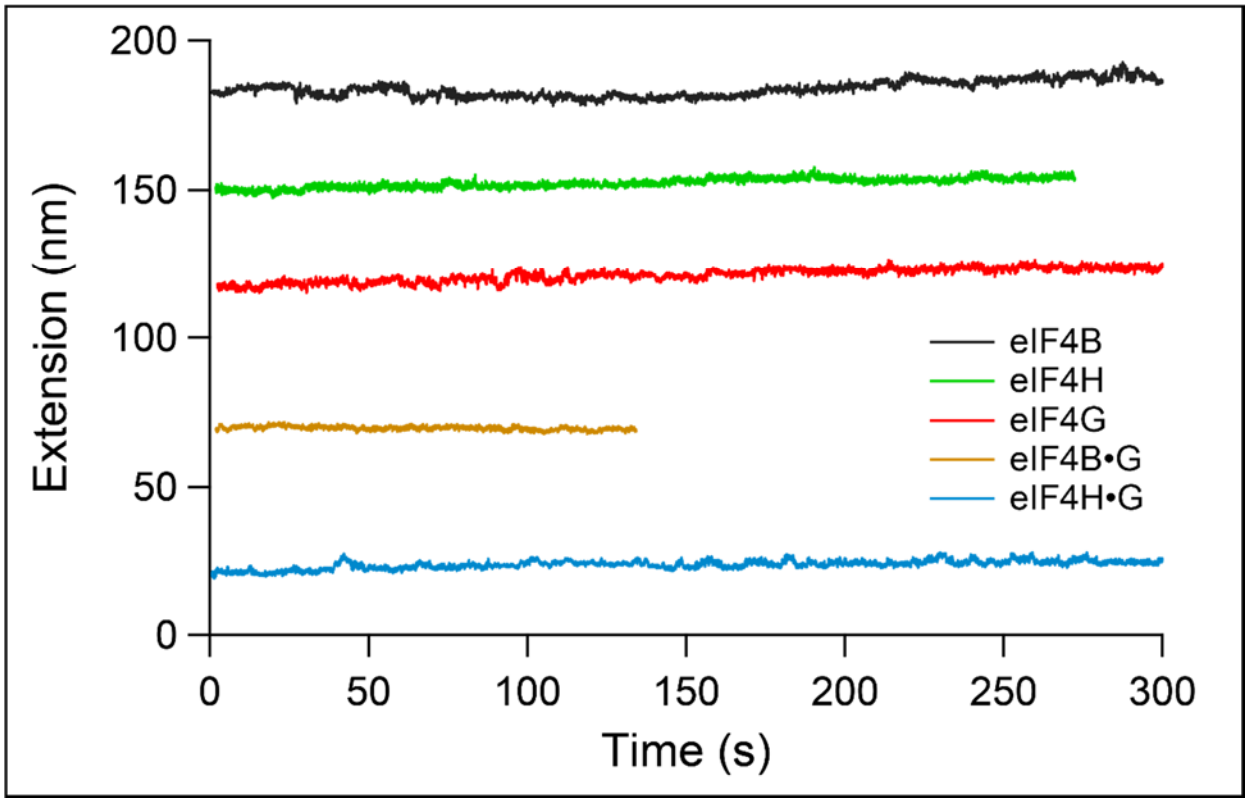

Fig. S4. Initiation factors eIF4B, eIF4H, and eIF4G and combinations thereof fail to unwind dsRNA in the absence of eIF4A.

To ensure that the unwinding activity was produced by eIF4A helicase in single-molecule assays, we ran controls with other combinations of initiation factors lacking the eIF4A protein. The figure shows representative records collected at 1 μM eIF4B (black), eIF4H (green), eIF4G$_{682\text{-}1105}$ (red), eIF4B•G$_{682\text{-}1105}$ (gold) and eIF4H•G$_{682\text{-}1105}$ (blue), none of which display unwinding activity. The traces are offset on the vertical axis for clarity.

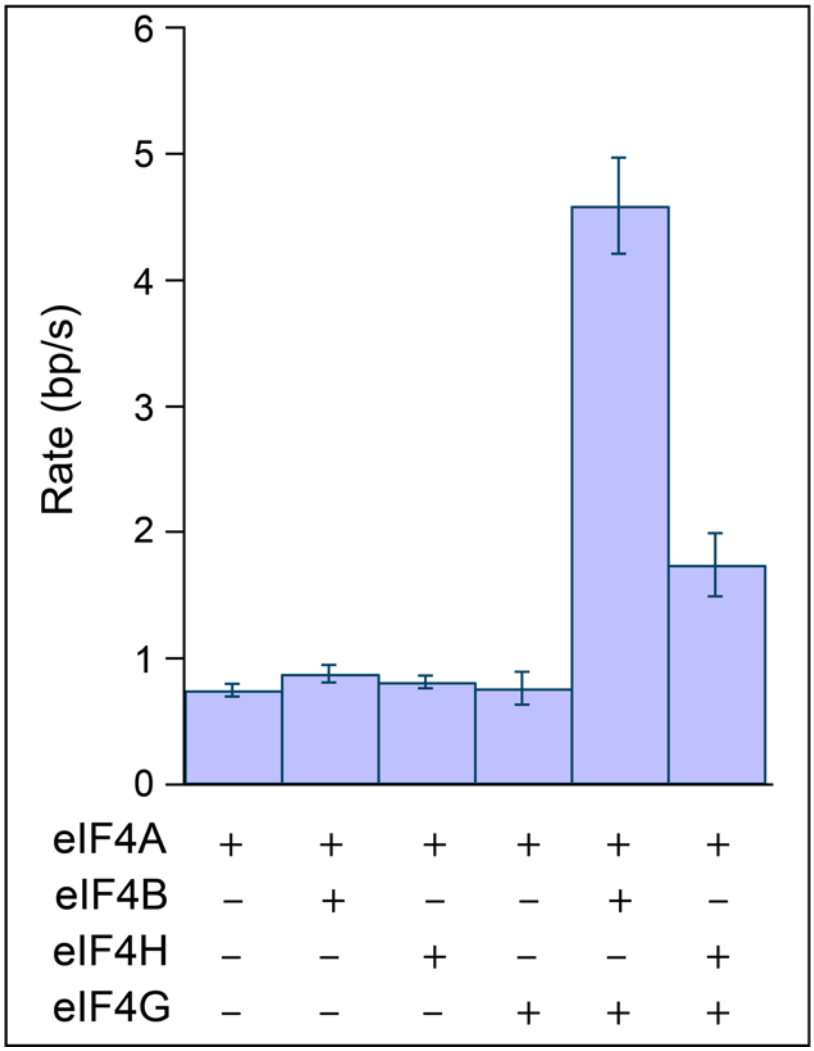

Fig. S5. Overall unwinding rates of eIF4A helicase alone or bound to different combinations of eIF4B, eIF4H and eIF4G.

Mean unwinding rates were calculated for each factor combination by averaging ratios of the net unwinding of the reporter hairpin (measured in bp) to the corresponding time required for that unwinding. Because the complexes eIF4A, eIF4A•B, eIF4A•H, and eIF4A•G only partially unwind the hairpin, followed by one or more episodes of re-annealing, their low apparent rates tend to reflect the unwinding achieved before complete hairpin refolding. Unwinding rates for eIF4A•B•G and eIF4A•B•G are larger, and therefore indicative of progressive unwinding. (The contribution of the final opening step, which is mediated by force, was not included in these estimates. Error bars, SEM.)

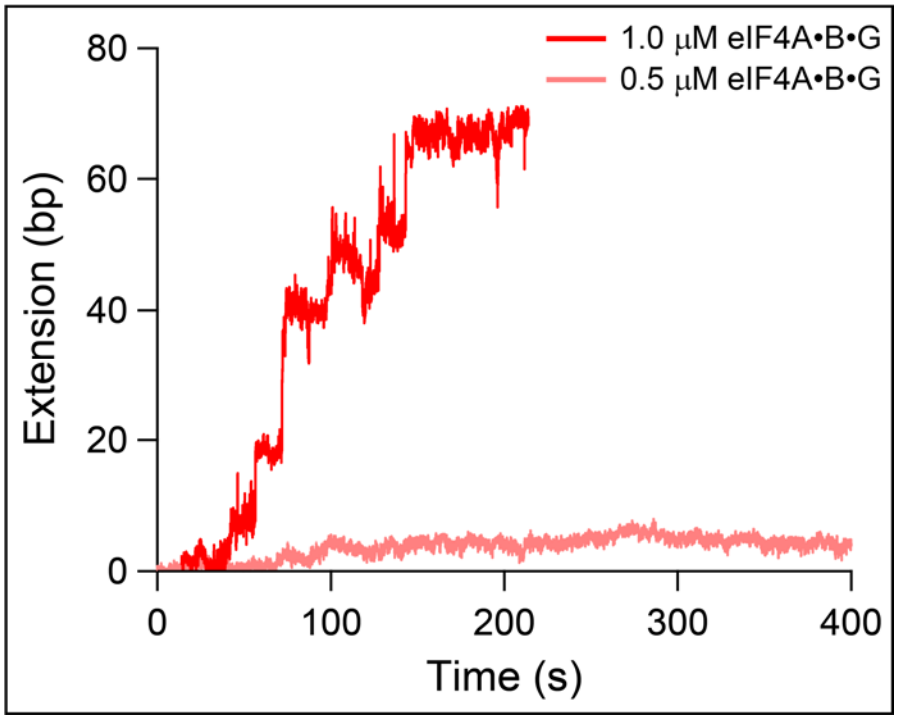

Fig. S6. Effect of nominal eIF4A•B•G concentration on activity.
Representative records of reporter hairpin unwinding for eIF4A•B•G collected on the same hairpin tether when nominal concentrations of 0.5 μM (pink trace) and then 1 μM (red trace) were introduced into the flow cell. There was no activity seen at 0.5 μM, consistent with general observations of loss of activity at concentrations of 0.5 μM and below and attributable to the low initial concentration and the adhesion of proteins introduced into the flowcell (see text).

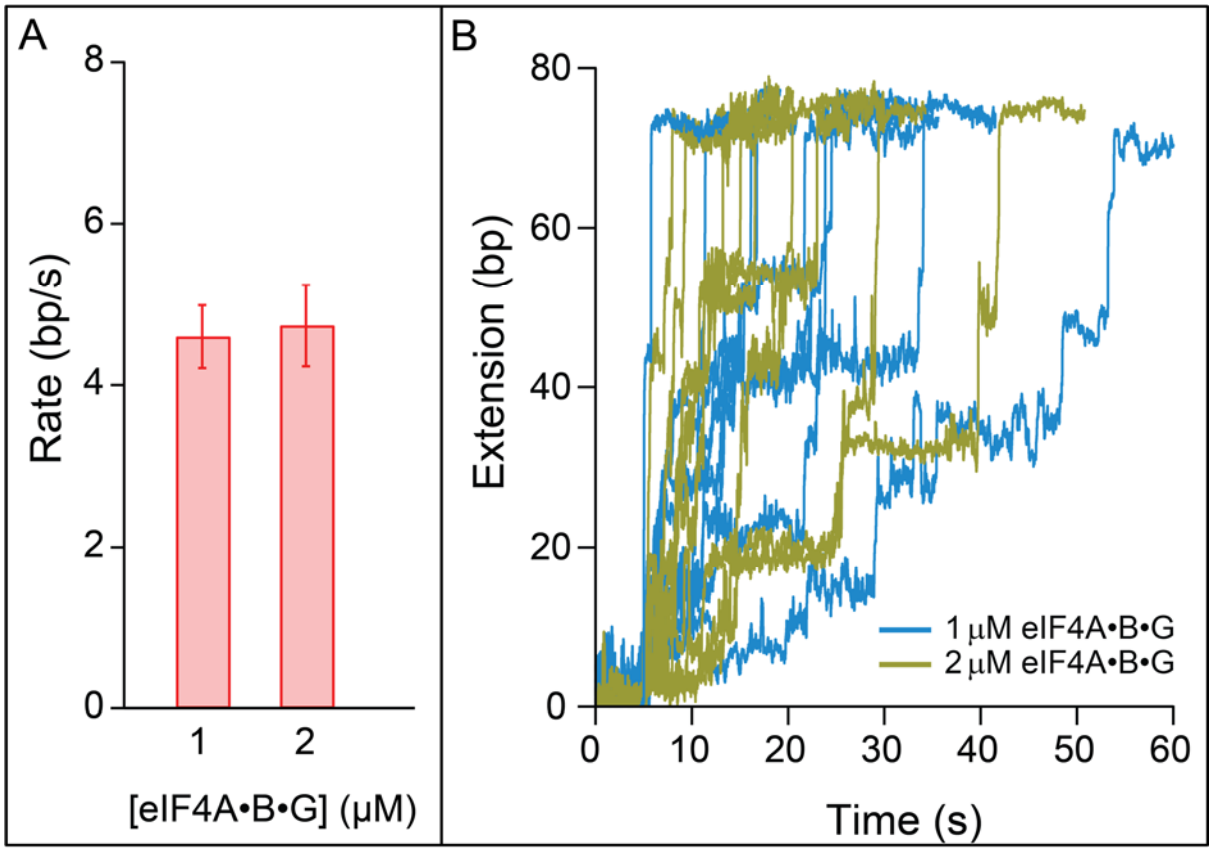

Fig. S7. eIF4A•B•G$_{682\text{-}1105}$ unwinding activity compared at 1 μM and 2 μM.
Reporter hairpin unwinding by the eIF4A•B•G$_{682\text{-}1105}$ complex at a nominal initial concentration of 1 μM (the standard condition used for these assays) compared with at 2 μM. (**A**) Overall unwinding rates scored, as in Figure S5, as the ratio of net base pairs unwound to the corresponding unwinding time, excluding the last opening event, which is mediated by force. The rates were statistically identical at the two different concentrations (4.6 ± 0.3 bp/s (N = 51) and 4.7 ± 0.5 bp/s (N = 9) (mean ± SEM) for concentrations of 1 and 2 μM eIF4A•B•G, respectively). (**B**) Representative single-molecule records obtained at 1 μM (blue traces) and 2 μM (olive traces). All records show complete unwinding of the hairpin in times ranging from 5-50 s. There was no evidence that unwinding proceeded faster at the higher concentration. These data support a processive, not distributive, mechanism for unwinding (see text).

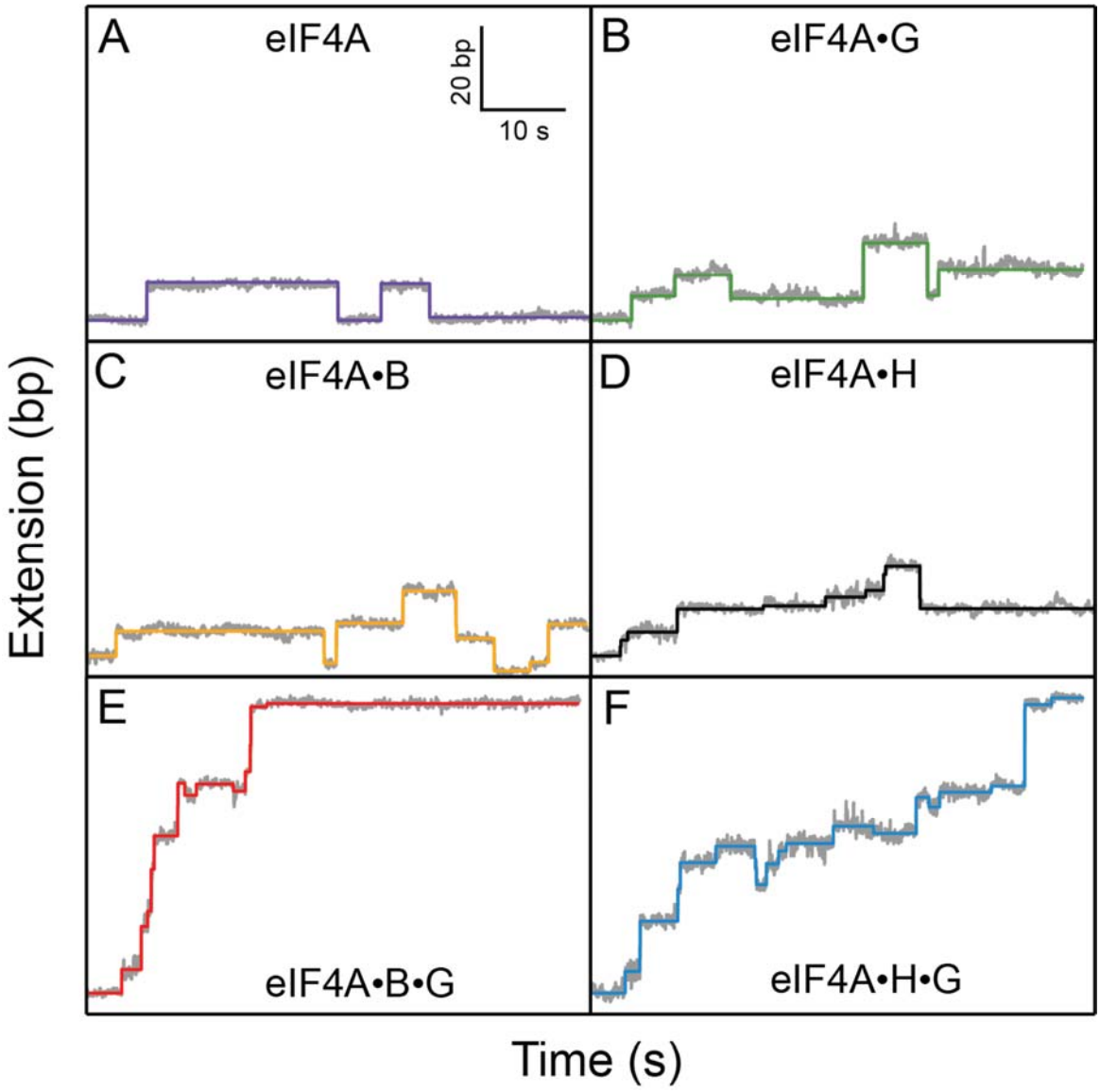

Fig. S8. Step-finding algorithm used to identify unwinding steps.

The figure displays representative records of reporter hairpin unwinding for each factor combination (data shown in grey) with the corresponding fits produced by the step-finding algorithm, superposed in color. (**A**) eIF4A (purple trace), (**B**) eIF4A•$G_{682\text{-}1105}$ (green trace), (**C**) eIF4A•B (yellow trace), (**D**) eIF4A•H (black trace), (**E**) eIF4A•B•$G_{682\text{-}1105}$ (red trace), (**F**) eIF4A•H•$G_{682\text{-}1105}$ (blue trace). To ensure that data were not under- or over-fit, we selected the number of steps producing a maximum in the "standard step indicator," *S*, which is the ratio, for an *n*-step fit, of the χ^2-squared value assuming a false fit (step locations offset) to the χ^2-squared value for the identified fit, according to (*28*).

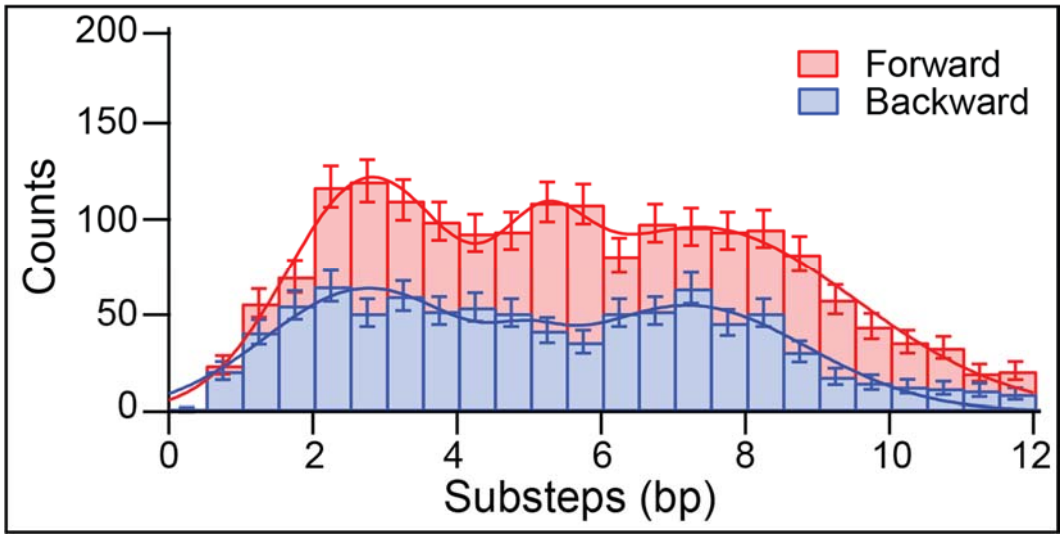

Fig. S9. Histogram of forward and backward substeps.

The 11 bp steps of eIF4A helicase and factor combinations generally showed a stepwise substructure. A step-finding algorithm (see Figure S3 and main text) was employed to estimate the sizes of any substeps (*28*); substeps could be resolved down to ~2-3 bp. Binning of substeps from all the factor combinations yielded a three-peaked distribution. The shape of the distribution was similar, regardless of whether the substeps in question were forward (red) or backward (blue). Fitting the forward distribution to a sum of three Gaussians yielded mean substep sizes of 2.7 ± 1.1, 5.2 ± 1.1, and 7.3 ± 1.3 bp; similarly, the backward distribution gave substep sizes of 2.7 ± 1.2, 5.0 ± 1.5, and 7.2 ± 1.3 bp (mean ± SEM). To confirm that a sum of three Gaussians, rather than one or two, best modeled the data, we calculated reduced chi-squared values, $\tilde{\chi}^2$, for each possible fit, and found that $\tilde{\chi}_1^2 \gg \tilde{\chi}_2^2 > \tilde{\chi}_3^2 \approx 2.7 > 1$, where the subscript indicates the number of Gaussians.

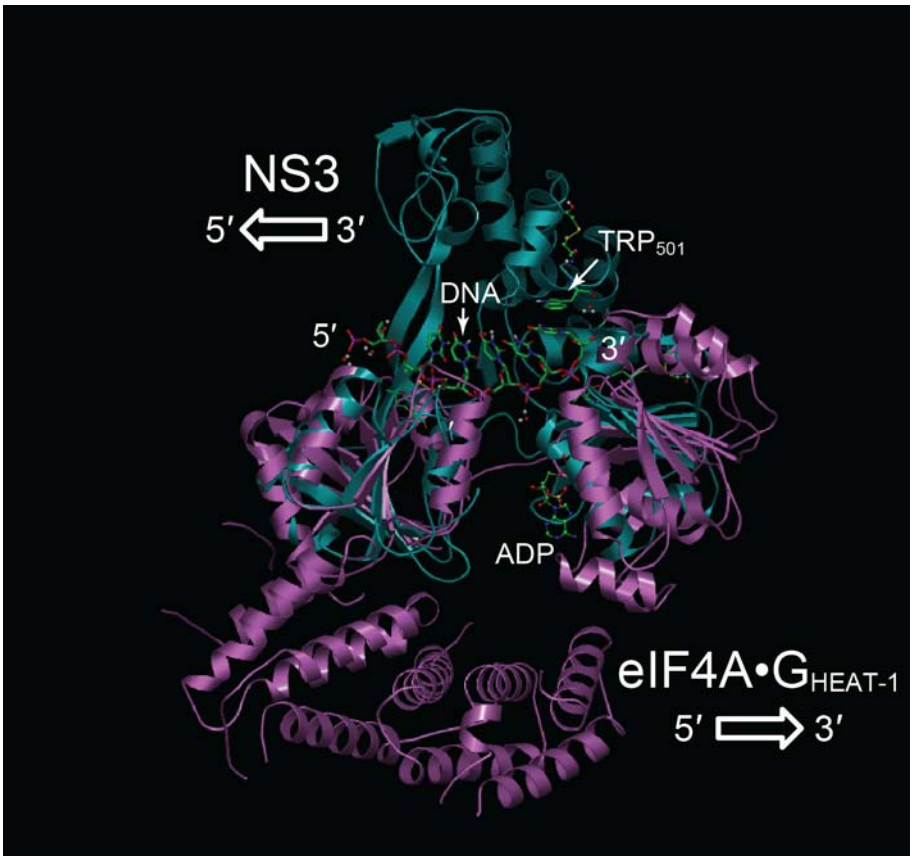

Fig. S10. eIF4A•G and NS3 3D sequence alignment.

The figure shows a three-dimensional sequence alignment of the complex eIF4A•G_{HEAT-1} (purple, PDB code 1HU3) and NS3 helicase (turquoise, PDB code 1A1V) (*48, 50*). The two RecA-like domains of eIF4A and NS3, NTD and CTD, align reasonably well. Interestingly, the HEAT-1 domain of eIF4G (bottom purple) "mirrors," rather than aligns directly, with domain 3 of NS3 (top, turquoise). The translocation directionality (white arrows) of these DEAD-box helicases differ in their native contexts (note that eIF4A must be complexed with additional factors to exhibit directionality). It has been suggested that TRP_{501}, located in NS3 domain 3, is the "gatekeeper" residue and prevents the nucleic acid template from "slipping" backwards in the 5′-to-3′ direction (*30*). However, no equivalent amino acid is found in the eIF4A•G_{HEAT-1} complex, perhaps explaining why we observed similar numbers of forward and backward steps (~1.7 ratio) for the eIF4A•$G_{682-1105}$ complex. (The $eIF4G_{682-1105}$ truncation contains the HEAT-1 domain plus two other domains for RNA and eIF3 binding).

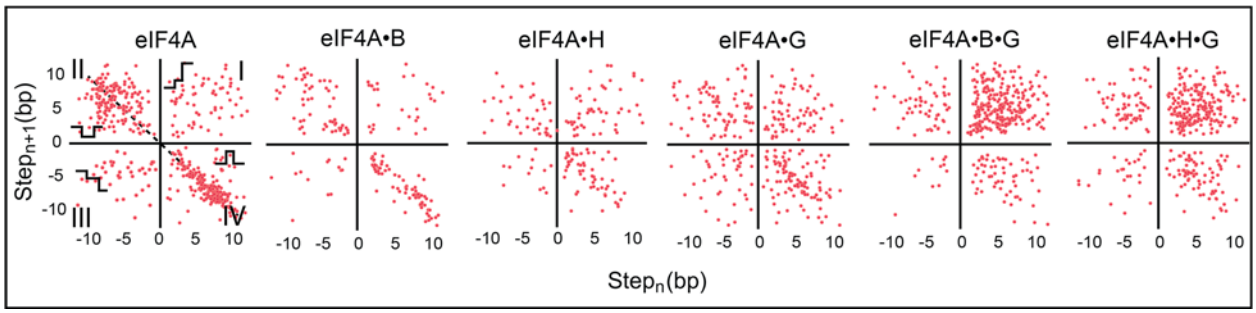

Fig. S11. Correlation between consecutive steps for each factor combination.

The plots show the correlation between size and direction of the current step (*step*$_n$, *x*-axis) and the subsequent step (*step*$_{n+1}$, *y*-axis) for the factor combinations indicated. Each of the quadrants represents a specific pattern of events: in the first quadrant (I), a forward step follows a forward step; in the second (II), a forward step follows a backward step; in the third (III), a backward step follows a backward step; and in the fourth (IV), a backward step follows a forward step. Points above the -45^0 line (dashed line) correspond to (net) 5′-to-3′ translocation; points below this line correspond to 3′-to-5′ translocation; points situated on the line do not lead to translocation. The dynamics of eIF4A alone (leftmost panel) are dominated by a step forward followed by a step backward (fourth quadrant) or by a step backward followed by a step forward (second quadrant). Roughly similar (but more scattered, and therefore less correlated) behavior was observed for the binary complexes eIF4A•B, eIF4A•H and IF4A•G. By contrast, for the ternary complexes eIF4A•B•G and eIF4A•H•G, the dynamics shifted to the first quadrant (a step forward followed by a step forward), reflecting the increased processivity of these combinations.

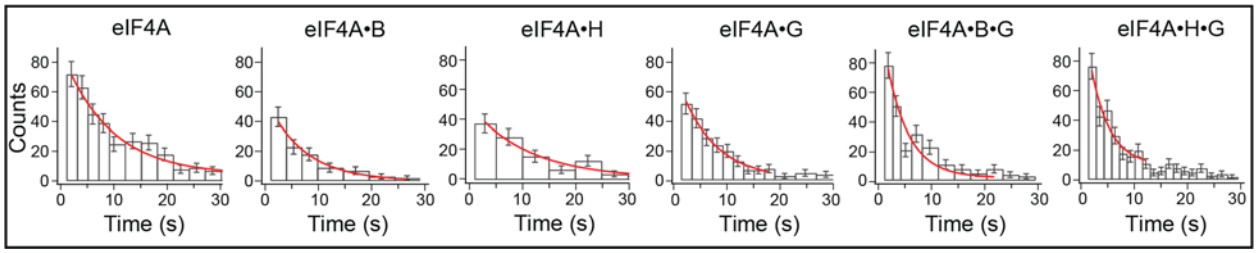

Fig. S12. Factor dependence of pausing.

Pause-duration histograms for eIF4A alone, or complexed with the factor combinations indicated. In each case, the data were well-fit by a single exponential, suggesting that translocation is governed by a single rate-limiting step. The enhanced processivity of eIF4A upon binding either eIF4B, eIF4H or eIF4G was accompanied by a decrease in the mean pause lifetime. Error bars, SE.

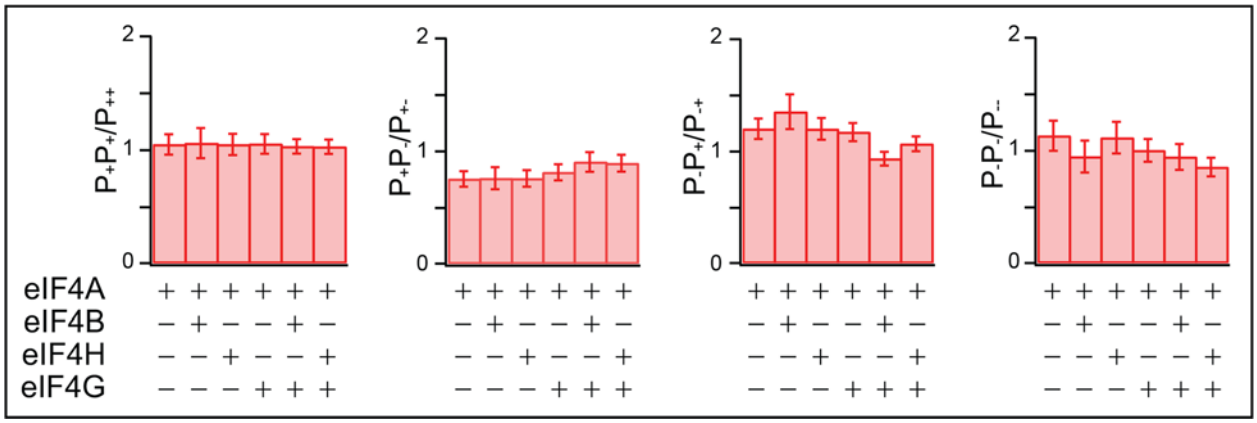

Fig. S13. Lack of memory in successive steps (Markov property).

The ratio P_+P_+/P_{++} (where P_+ is the probability of a forward step and P_{++} is the probability of two consecutive forward steps; see text) evaluates the independence of two forward steps and was near unity for each of the factor combinations indicated (legend, leftmost panel). Similarly, the ratios P_+P_-/P_{+-}, P_-P_+/P_{-+}, and P_-P_-/P_{--} (where P_- is the probability of taking a backward step and P_{+-}, P_{-+}, P_{--} are the probabilities of consecutive forward and/or backward steps; see text) were approximately equal to one, indicating that the helicase complexes exhibit little or no memory of the preceding step. Error bars, SEM.

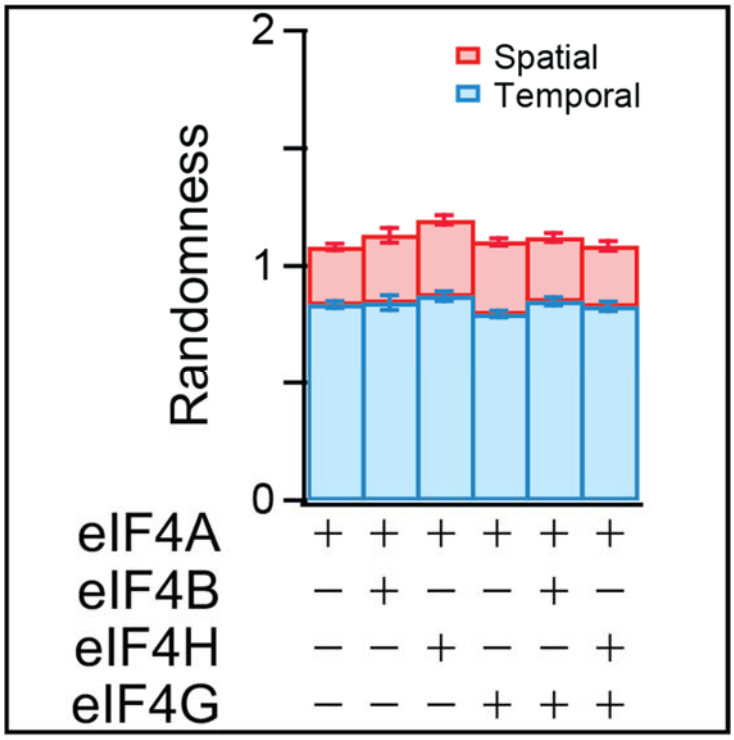

Fig. S14. Calculated randomness implies one rate-limiting step.

The total randomness parameter (spatial plus temporal), *r*, was calculated for each complex (see text). Independent of the factor combination, the randomness was found to be approximately one, suggesting that there is only a single rate-limiting step in the translocation of eIF4A, regardless of the initiation factors bound to it. Error bars, SEM.

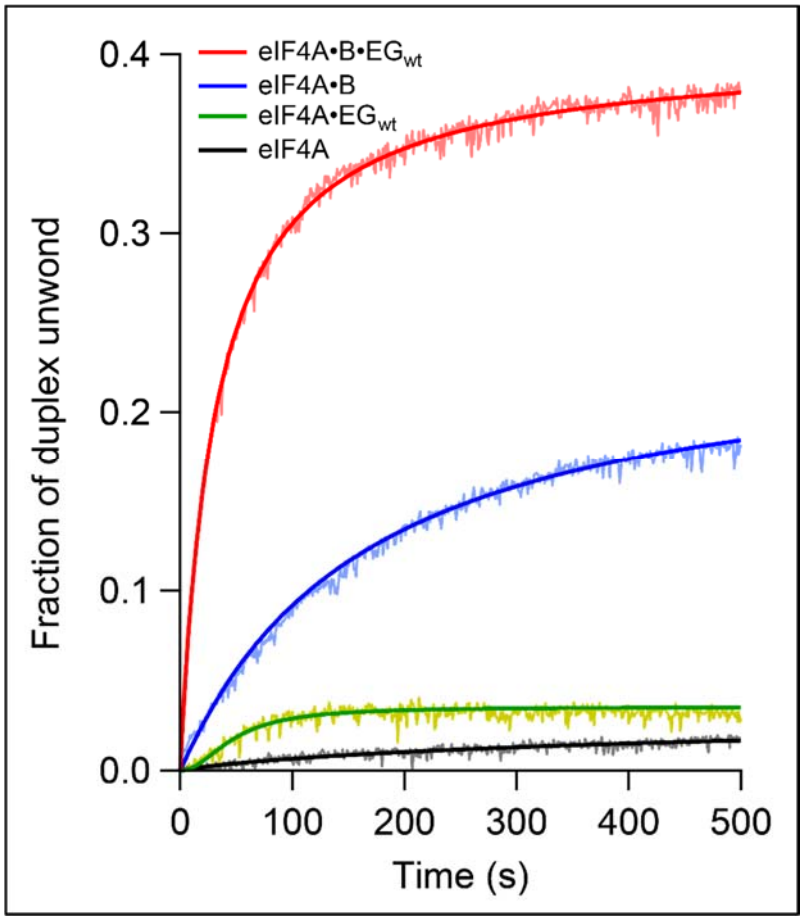

Fig. S15. Enhancement of eIF4A helicase activity by factors eIF4B and eIF4EG$_{wt}$.
The importance of additional factors on eIF4A unwinding activity was tested in a bulk fluorescence-based assay, as described (*51*). Representative time courses for unwinding (expressed as fraction of total RNA duplex unwound) are shown for eIF4A alone (black) or in the presence of eIF4B (blue), eIF4G and eIF4E (green), or eIF4B, eIF4G$_{wt}$ and eIF4E (red). Unwinding activity was greatest for eIF4A•B•EG$_{wt}$, and decreased for other partial factor combinations; for example, eIF4A•EG$_{wt}$ activity was relatively negligible without eIF4B. Note that relative activities reported here with eIF4G$_{wt}$ agree well with those previously reported with the truncation mutant used elsewhere in this work (eIF4G$_{682-1105}$).

Factor combination	Arrival time ± SEM (s)
eIF4A	69 ± 10
eIF4A•B	67 ± 12
eIF4A•H	66 ± 10
eIF4A•$G_{682\text{-}1105}$	35 ± 8
eIF4A•B•$G_{682\text{-}1105}$	29 ± 4
eIF4A•H•$G_{682\text{-}1105}$	34 ± 4

Table S1. Arrival times for different initiation factor combinations.

The arrival time was operationally defined as the interval, in seconds, between the introduction of a protein factor (or factor combination) into the microscope flow cell and the first detectable change in tether length of the reporter hairpin, minus the time required to complete the buffer exchange (taken to be 5 ± 1 s, mean ± SE, based on measurements by dye exchange and mechanical settling time). Arrival times therefore reflect the time required for initiation factors to find their RNA target, bind, and become enzymatically active in unwinding.

REFERENCES

1. A. Parsyan, Y. Svitkin, D. Shahbazian, C. Gkogkas, P. Lasko, W. C. Merrick, N. Sonenberg, mRNA helicases: The tacticians of translational control. *Nat. Rev. Mol. Cell Biol.* **12**, 235–245 (2011). Medline doi:10.1038/nrm3083

2. P. Linder, E. Jankowsky, From unwinding to clamping - the DEAD box RNA helicase family. *Nat. Rev. Mol. Cell Biol.* **12**, 505–516 (2011). Medline doi:10.1038/nrm3154

3. I. Jarmoskaite, R. Russell, RNA helicase proteins as chaperones and remodelers. *Annu. Rev. Biochem.* **83**, 697–725 (2014). Medline doi:10.1146/annurev-biochem-060713-035546

4. S. Rocak, P. Linder, DEAD-box proteins: The driving forces behind RNA metabolism. *Nat. Rev. Mol. Cell Biol.* **5**, 232–241 (2004). Medline doi:10.1038/nrm1335

5. I. Jarmoskaite, R. Russell, DEAD-box proteins as RNA helicases and chaperones. *Wiley Interdiscip. Rev.: RNA* **2**, 135–152 (2011). Medline doi:10.1002/wrna.50

6. S. A. Woodson, Taming free energy landscapes with RNA chaperones. *RNA Biol.* **7**, 677–686 (2010). Medline doi:10.4161/rna.7.6.13615

7. M. E. Fairman-Williams, U.-P. Guenther, E. Jankowsky, SF1 and SF2 helicases: Family matters. *Curr. Opin. Struct. Biol.* **20**, 313–324 (2010). Medline doi:10.1016/j.sbi.2010.03.011

8. J. M. Caruthers, E. R. Johnson, D. B. McKay, Crystal structure of yeast initiation factor 4A, a DEAD-box RNA helicase. *Proc. Natl. Acad. Sci. U.S.A.* **97**, 13080–13085 (2000). Medline doi:10.1073/pnas.97.24.13080

9. C. E. Aitken, J. R. Lorsch, A mechanistic overview of translation initiation in eukaryotes. *Nat. Struct. Mol. Biol.* **19**, 568–576 (2012). Medline doi:10.1038/nsmb.2303

10. A. Marintchev, K. A. Edmonds, B. Marintcheva, E. Hendrickson, M. Oberer, C. Suzuki, B. Herdy, N. Sonenberg, G. Wagner, Topology and regulation of the human eIF4A/4G/4H helicase complex in translation initiation. *Cell* **136**, 447–460 (2009). Medline doi:10.1016/j.cell.2009.01.014

11. K. H. Nielsen, M. A. Behrens, Y. He, C. L. Oliveira, L. S. Jensen, S. V. Hoffmann, J. S. Pedersen, G. R. Andersen, Synergistic activation of eIF4A by eIF4B and eIF4G. *Nucleic Acids Res.* **39**, 2678–2689 (2011). Medline doi:10.1093/nar/gkq1206

12. Y. Sun, E. Atas, L. Lindqvist, N. Sonenberg, J. Pelletier, A. Meller, The eukaryotic initiation factor eIF4H facilitates loop-binding, repetitive RNA unwinding by the eIF4A DEAD-box helicase. *Nucleic Acids Res.* **40**, 6199–6207 (2012). Medline doi:10.1093/nar/gks278

13. R. D. Abramson, T. E. Dever, W. C. Merrick, Biochemical evidence supporting a mechanism for cap-independent and internal initiation of eukaryotic mRNA. *J. Biol. Chem.* **263**, 6016–6019 (1988). Medline

14. Y. Sun, E. Atas, L. M. Lindqvist, N. Sonenberg, J. Pelletier, A. Meller, Single-molecule kinetics of the eukaryotic initiation factor 4AI upon RNA unwinding. *Structure* **22**, 941–948 (2014). Medline doi:10.1016/j.str.2014.04.014

15. F. Liu, A. Putnam, E. Jankowsky, ATP hydrolysis is required for DEAD-box protein recycling but not for duplex unwinding. *Proc. Natl. Acad. Sci. U.S.A.* **105**, 20209–20214 (2008). Medline doi:10.1073/pnas.0811115106

16. M. Kozak, The scanning model for translation: An update. *J. Cell Biol.* **108**, 229–241 (1989). Medline doi:10.1083/jcb.108.2.229

17. A. Z. Andreou, D. Klostermeier, The DEAD-box helicase eIF4A: Paradigm or the odd one out? *RNA Biol.* **10**, 19–32 (2013). Medline doi:10.4161/rna.21966

18. E. De Gregorio, T. Preiss, M. W. Hentze, Translation driven by an eIF4G core domain in vivo. *EMBO J.* **18**, 4865–4874 (1999). Medline doi:10.1093/emboj/18.17.4865

19. K. Feoktistova, E. Tuvshintogs, A. Do, C. S. Fraser, Human eIF4E promotes mRNA restructuring by stimulating eIF4A helicase activity. *Proc. Natl. Acad. Sci. U.S.A.* **110**, 13339–13344 (2013). Medline doi:10.1073/pnas.1303781110

20. N. L. Korneeva, E. A. First, C. A. Benoit, R. E. Rhoads, Interaction between the NH2-terminal domain of eIF4A and the central domain of eIF4G modulates RNA-stimulated ATPase activity. *J. Biol. Chem.* **280**, 1872–1881 (2005). Medline doi:10.1074/jbc.M406168200

21. J. R. Lorsch, D. Herschlag, The DEAD box protein eIF4A. 2. A cycle of nucleotide and RNA-dependent conformational changes. *Biochemistry* **37**, 2194–2206 (1998). Medline doi:10.1021/bi9724319

22. M. L. Peck, D. Herschlag, Effects of oligonucleotide length and atomic composition on stimulation of the ATPase activity of translation initiation factor elF4A. *RNA* **5**, 1210–1221 (1999). Medline doi:10.1017/S1355838299990817

23. F. Rozen, I. Edery, K. Meerovitch, T. E. Dever, W. C. Merrick, N. Sonenberg, Bidirectional RNA helicase activity of eucaryotic translation initiation factors 4A and 4F. *Mol. Cell. Biol.* **10**, 1134–1144 (1990). Medline

24. G. W. Rogers Jr., N. J. Richter, W. F. Lima, W. C. Merrick, Modulation of the helicase activity of eIF4A by eIF4B, eIF4H, and eIF4F. *J. Biol. Chem.* **276**, 30914–30922 (2001). Medline doi:10.1074/jbc.M100157200

25. G. W. Rogers Jr., N. J. Richter, W. C. Merrick, Biochemical and kinetic characterization of the RNA helicase activity of eukaryotic initiation factor 4A. *J. Biol. Chem.* **274**, 12236–12244 (1999). Medline doi:10.1074/jbc.274.18.12236

26. A. Z. Andreou, D. Klostermeier, eIF4B and eIF4G jointly stimulate eIF4A ATPase and unwinding activities by modulation of the eIF4A conformational cycle. *J. Mol. Biol.* **426**, 51–61 (2014). Medline

27. M. J. Schnitzer, S. M. Block, Kinesin hydrolyses one ATP per 8-nm step. *Nature* **388**, 386–390 (1997). Medline doi:10.1038/41111

28. J. W. J. Kerssemakers, E. L. Munteanu, L. Laan, T. L. Noetzel, M. E. Janson, M. Dogterom, Assembly dynamics of microtubules at molecular resolution. *Nature* **442**, 709–712 (2006). Medline doi:10.1038/nature04928

29. A. M. Pyle, Translocation and unwinding mechanisms of RNA and DNA helicases. *Annu. Rev. Biophys.* **37**, 317–336 (2008). Medline doi:10.1146/annurev.biophys.37.032807.125908

30. S. Myong, M. M. Bruno, A. M. Pyle, T. Ha, Spring-loaded mechanism of DNA unwinding by hepatitis C virus NS3 helicase. *Science* **317**, 513–516 (2007). Medline doi:10.1126/science.1144130

31. K. L. Frieda, S. M. Block, Direct observation of cotranscriptional folding in an adenine riboswitch. *Science* **338**, 397–400 (2012). Medline doi:10.1126/science.1225722

32. W. J. Greenleaf, K. L. Frieda, D. A. Foster, M. T. Woodside, S. M. Block, Direct observation of hierarchical folding in single riboswitch aptamers. *Science* **319**, 630–633 (2008). Medline doi:10.1126/science.1151298

33. A. R. Özeş, K. Feoktistova, B. C. Avanzino, C. S. Fraser, Duplex unwinding and ATPase activities of the DEAD-box helicase eIF4A are coupled by eIF4G and eIF4B. *J. Mol. Biol.* **412**, 674–687 (2011). Medline doi:10.1016/j.jmb.2011.08.004

34. J. R. Lorsch, D. Herschlag, The DEAD box protein eIF4A. 1. A minimal kinetic and thermodynamic framework reveals coupled binding of RNA and nucleotide. *Biochemistry* **37**, 2180–2193 (1998). Medline doi:10.1021/bi972430g

35. B. E. Clancy, W. M. Behnke-Parks, J. O. Andreasson, S. S. Rosenfeld, S. M. Block, A universal pathway for kinesin stepping. *Nat. Struct. Mol. Biol.* **18**, 1020–1027 (2011). Medline doi:10.1038/nsmb.2104

36. J. W. Shaevitz, S. M. Block, M. J. Schnitzer, Statistical kinetics of macromolecular dynamics. *Biophys. J.* **89**, 2277–2285 (2005). Medline doi:10.1529/biophysj.105.064295

37. K. M. Herbert, A. La Porta, B. J. Wong, R. A. Mooney, K. C. Neuman, R. Landick, S. M. Block, Sequence-resolved detection of pausing by single RNA polymerase molecules. *Cell* **125**, 1083–1094 (2006). Medline doi:10.1016/j.cell.2006.04.032

38. V. M. Weake, J. L. Workman, Inducible gene expression: Diverse regulatory mechanisms. *Nat. Rev. Genet.* **11**, 426–437 (2010). Medline doi:10.1038/nrg2781

39. J. W. Hershey, Translational control in mammalian cells. *Annu. Rev. Biochem.* **60**, 717–755 (1991). Medline doi:10.1146/annurev.bi.60.070191.003441

40. D. R. Cavener, Comparison of the consensus sequence flanking translational start sites in Drosophila and vertebrates. *Nucleic Acids Res.* **15**, 1353–1361 (1987). Medline doi:10.1093/nar/15.4.1353

41. M. Kozak, Compilation and analysis of sequences upstream from the translational start site in eukaryotic mRNAs. *Nucleic Acids Res.* **12**, 857–872 (1984). Medline doi:10.1093/nar/12.2.857

42. M. Kozak, Point mutations define a sequence flanking the AUG initiator codon that modulates translation by eukaryotic ribosomes. *Cell* **44**, 283–292 (1986). Medline doi:10.1016/0092-8674(86)90762-2

43. M. Kozak, At least six nucleotides preceding the AUG initiator codon enhance translation in mammalian cells. *J. Mol. Biol.* **196**, 947–950 (1987). Medline doi:10.1016/0022-2836(87)90418-9

44. R. J. Jackson, C. U. Hellen, T. V. Pestova, The mechanism of eukaryotic translation initiation and principles of its regulation. *Nat. Rev. Mol. Cell Biol.* **11**, 113–127 (2010). Medline doi:10.1038/nrm2838

45. X. Qu, L. Lancaster, H. F. Noller, C. Bustamante, I. Tinoco Jr., Ribosomal protein S1 unwinds double-stranded RNA in multiple steps. *Proc. Natl. Acad. Sci. U.S.A.* **109**, 14458–14463 (2012). Medline doi:10.1073/pnas.1208950109

46. V. Rajagopal, E.-H. Park, A. G. Hinnebusch, J. R. Lorsch, Specific domains in yeast translation initiation factor eIF4G strongly bias RNA unwinding activity of the eIF4F complex toward duplexes with 5′-overhangs. *J. Biol. Chem.* **287**, 20301–20312 (2012). Medline doi:10.1074/jbc.M112.347278

47. G. W. Rogers Jr., A. A. Komar, W. C. Merrick, eIF4A: The godfather of the DEAD box helicases. *Prog. Nucleic Acid Res. Mol. Biol.* **72**, 307–331 (2002). Medline

48. P. Schütz, M. Bumann, A. E. Oberholzer, C. Bieniossek, H. Trachsel, M. Altmann, U. Baumann, Crystal structure of the yeast eIF4A-eIF4G complex: An RNA-helicase controlled by protein-protein interactions. *Proc. Natl. Acad. Sci. U.S.A.* **105**, 9564–9569 (2008). Medline doi:10.1073/pnas.0800418105

49. M. Zuker, Mfold web server for nucleic acid folding and hybridization prediction. *Nucleic Acids Res.* **31**, 3406–3415 (2003). Medline doi:10.1093/nar/gkg595

50. J. L. Kim, K. A. Morgenstern, C. Lin, T. Fox, M. D. Dwyer, J. A. Landro, S. P. Chambers, W. Markland, C. A. Lepre, E. T. O'Malley, S. L. Harbeson, C. M. Rice, M. A. Murcko, P. R. Caron, J. A. Thomson, Crystal structure of the hepatitis C virus NS3 protease domain complexed with a synthetic NS4A cofactor peptide. *Cell* **87**, 343–355 (1996). Medline doi:10.1016/S0092-8674(00)81351-3

51. A. R. Özeş, K. Feoktistova, B. C. Avanzino, E. P. Baldwin, C. S. Fraser, Real-time fluorescence assays to monitor duplex unwinding and ATPase activities of helicases. *Nat. Protoc.* **9**, 1645–1661 (2014). Medline doi:10.1038/nprot.2014.112